THE JOURNAL OF PHYSICAL CHEMISTRY C

Article

pubs.acs.org/JPCC

Simultaneous Sheet Cross-Linking and Deoxygenation in the Graphene Oxide Sol–Gel Transition

Anna P. Goldstein,[†,‡] William Mickelson,[§,∥] Ariella Machness,[∥] Gloria Lee,[§] Marcus A. Worsley,[⊥] Leta Woo,[⊥] and Alex Zettl*[,‡,§,∥,#]

[†]Department of Chemistry and [§]Department of Physics, University of California, Berkeley, California 94720, United States

[‡]Materials Science Division, Lawrence Berkeley National Laboratory, Berkeley, California 94720, United States

[∥]Center of Integrated Nanomechanical Systems, Berkeley, California 94720, United States

[⊥]Physical and Life Sciences Directorate, Lawrence Livermore National Laboratory, Livermore, California 94550, United States

[#]Kavli Energy NanoSciences Institute at Berkeley, Berkeley, California 94720, United States

Supporting Information

ABSTRACT: The precursor material to graphene aerogels is a hydrogel formed from an aqueous solution of graphene oxide. We investigate the time evolution of the physical and chemical properties of a graphene oxide suspension as it transitions to a hydrogel. Fully formed hydrogels undergo densification during reaction, forming mechanically stable monoliths. We demonstrate that the gelation process removes oxygen functional groups, partially re-forms the sp^2 network, and creates bonds between graphene oxide sheets. Furthermore, these changes to the physical and chemical properties occur on exactly the same time scale, suggesting that they have a common origin. This discovery lends greater understanding to the formation of graphene oxide-based hydrogels, which could allow more flexibility and tunability in synthetic methods for graphene-like materials.

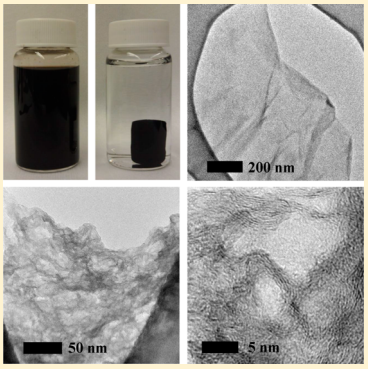

INTRODUCTION

Carbon aerogels are a promising class of lightweight materials with widespread potential applications, including oil adsorption and electrochemical energy storage.[1−3] Porous graphene has been suggested for possible use in water remediation,[4] gas sensing,[5] and electrochemical devices.[6] In general, graphene-based aerogels are three-dimensional porous structures composed of single- or few-layer graphene sheets, imparting such extraordinary graphene-like properties as large surface areas, supercompressibility, and high electrical conductivity.[7,8]

A number of synthesis methods have been proposed for graphene-based aerogels,[3,9−13] but the most common remains the sol–gel process, in which a solution (or suspension) of graphene oxide (GO) sheets is induced to react and form a solid network within a liquid phase. The liquid phase is then removed, typically by critical-point drying, followed by thermal annealing. Previous studies have shown that gelation of GO sheets can be accomplished across a range of temperatures utilizing its native chemical functionality, with or without addition of base.[7,14] Sol–gel chemistry has been thoroughly investigated for a wide range of chemical systems.[15−17] However, although some work has examined how various small molecules, polymers, and ions can act as cross-linkers in GO hydrogels,[9] the sol–gel chemistry of pure GO systems remains relatively unexplored.

Given GO's broad acceptance as a precursor for carbon aerogels, a better understanding of the GO sol–gel transition is warranted. Such an understanding is fundamental to precise chemical manipulation of GO sheets in solution and the realization of GO-based aerogels with controllable properties. The chemical structure of GO, based on the Lerf–Klinowski model,[18] consists primarily of a carbon network decorated with hydroxyls and 1,2-epoxides. Erickson et al. directly observed these groups within a sheet of GO using atomic-resolution transmission electron microscopy (TEM).[19] Previous work by Worsley et al. showed that, upon gelation, the peaks from hydroxyl, epoxide, and carboxyl groups in the ^{13}C NMR spectrum of GO disappear.[7,12] Meanwhile, a peak emerges upfield in the spectrum of gelled GO corresponding to the presence of sp^3-bonded carbon in methylene groups, similar to those observed in cross-linked organic sol–gels.[17] This suggests that covalent linkages between sheets are responsible for the formation of a hydrogel from GO. However, others have speculated that GO sheets are bound together by $\pi-\pi$ stacking,[14] so there is not yet a consensus on the bonding mechanism responsible for gelation.

Chemical reduction and thermal reduction impact many properties of GO, including enhanced conductivity and decreased ability to disperse in aqueous solution. GO can be

Received: September 11, 2014
Revised: November 7, 2014

   dx.doi.org/10.1021/jp5092027 | J. Phys. Chem. C XXXX, XXX, XXX−XXX

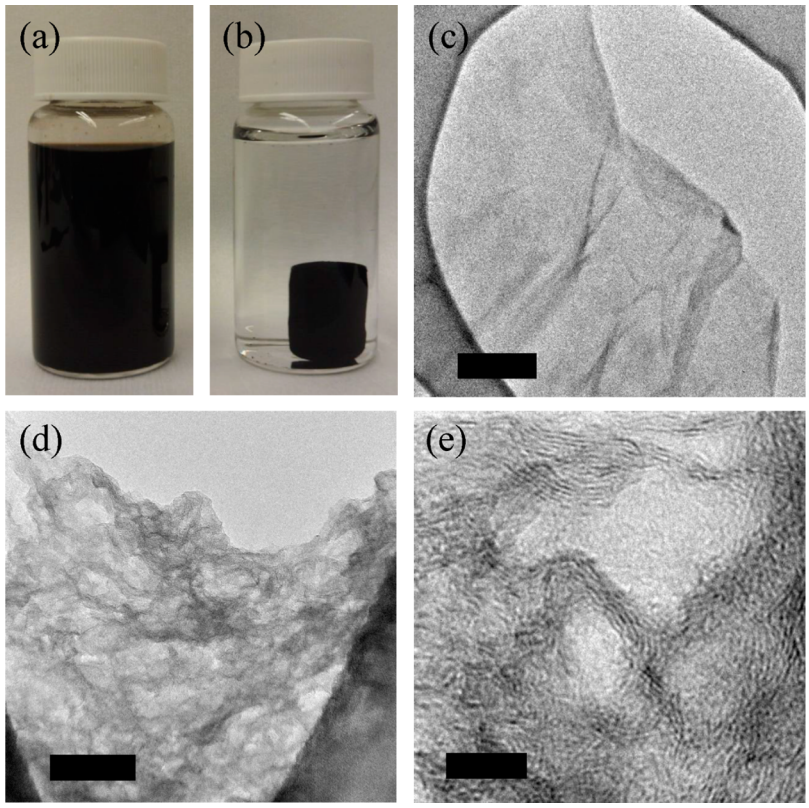

Figure 1. Photographs of (a) GO solution and (b) a formed hydrogel inside a 20 mL vial and (c–e) representative TEM images of hydrogel reacted for (c) 60 and (d,e) 90 min. Scale bars are (c) 200, (d) 50, and (e) 5 nm.

thermally reduced, or it can be chemically reduced by treatment with reducing agents, such as hydrazine and ammonia.[20−22] Many authors use reduced graphene oxide as an analogue for graphene. Prior publications on the gelation of GO also used this convention, referring to aerogels following thermal annealing as "graphene aerogels".[3,8] Because most of the characterization work has focused on annealed aerogels, much less is known about the intermediate product between graphene oxide and graphene aerogel. Here, we more thoroughly investigate the gelation of graphene oxide in order to identify the key chemical and physical changes responsible for the sol–gel transition in pure GO systems. By characterizing GO at various time points during the transition from GO solution to a sol–gel, we show that a number of changes in the physical, chemical, and optical properties emerge simultaneously upon gelation.

EXPERIMENTAL SECTION

Hydrothermal Synthesis. Graphene oxide (single-layer graphene oxide, Cheap Tubes, Inc.) was dispersed in deionized water by overnight bath sonication of 10–20 mg/mL solutions, resulting in a dark brown viscous suspension. These GO solutions were placed inside Teflon-lined pressure vessels from Parr Instrument Company preheated to 180 °C. Based on the measured heating rate inside an empty vessel, we estimate that approximately 45–60 min elapsed before the solution reached the reaction temperature. The vessels were removed from the heat after different time periods up to 18 h. Samples reacted for longer than 90 min were dried using a manual supercritical CO_2 dryer from Structure Probe, Inc., and some dried samples were annealed by heating to 1050 °C in a tube furnace under a nitrogen flow for 2 h.

Characterization. X-ray photoelectron spectroscopy (XPS) was performed using an Omicron EA 125 system with a monochromated Al source at 1486.6 eV. Samples were sonicated and dropcast on a Au thin film, and the Au 4f peak was used to verify the binding energy. Energy-dispersive X-ray spectroscopy (EDS) data were collected using an EDAX Genesis 2000 X-ray analyzer. Thermogravimetric analysis (TGA) data were collected using a TGA 7 instrument from Perkin-Elmer. Samples were heated at 10 °C/min in a 4:1 mixture of Ar and O_2. TEM characterization was performed using a JEOL 2010 microscope at 80 kV.

UV–visible (UV–vis) absorption spectra were collected using a Genesys 10S spectrometer from Thermo Scientific. Graphene oxide and the 60-min sample were sonicated for approximately 10 s before UV–vis analysis; other samples were sonicated for 2–3 min to create a stable suspension. Not all solid material was suspended; thus, the solutions were of unknown concentration.

RESULTS AND DISCUSSION

After undergoing heat treatment within the pressure vessel, the samples are visually inspected to assess any macroscopic changes to the GO solution. Samples reacted for 60 min or less remain as a dark brown solution, similar to the starting GO solution but with higher viscosity (Figure 1a). Samples reacted for 90 min or longer undergo a dramatic transition from a brown solution to a black hydrogel, which takes on the shape of the reaction vessel, but is approximately 50% smaller in each dimension (Figure 1b).

Characterization by TEM shows that the changes in macroscopic physical structure of the samples are also reflected on the nanoscale. Samples reacted for 60 min or less resemble

dx.doi.org/10.1021/jp5092027 | J. Phys. Chem. C XXXX, XXX, XXX–XXX

the starting GO material on the ~10−50-nm size scale. That is, they consist mostly of thin, featureless sheets, as seen in Figure 1c. In stark contrast to this morphology, samples reacted for 90 min or longer have no smooth portions; the entire sample is composed of a heavily textured matrix with high curvature and nanoscale pore structure, as shown in Figure 1d,e. The fact that, upon gelation, the two-dimensional GO sheets develop three-dimensional nanoscale features suggests that chemical bonding is changed throughout the entire GO sheet, not only at the edges. Additionally, the change in morphology suggests that bonds form between different GO sheets after approximately 75 min of reaction time, as the crumpling of the sheets causes a simultaneous macroscopic shrinkage of the gel.

As the gel is undergoing physical wrinkling and shrinkage, XPS data show clear signs of the chemical changes taking place during gelation. Figure 2 shows the carbon K-edge of the XPS

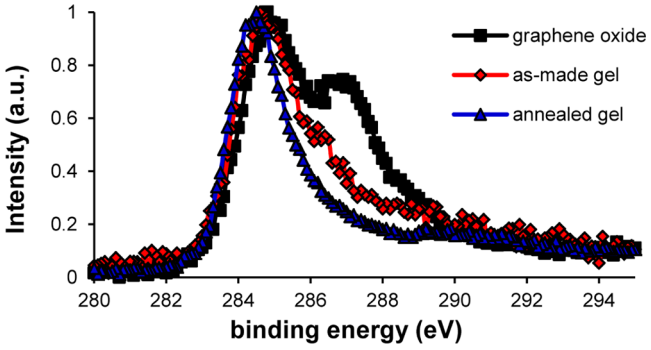

Figure 2. XPS of GO before gelation, after gelation, and after thermal annealing. Spectra are normalized at the maximum signal and baseline-subtracted.

spectrum for the GO starting material, a sample after gelation, and a sample that has been annealed at 1050 °C in nitrogen after undergoing gelation. The carbon K-edge for the GO starting material agrees with previously reported spectra for GO,[23] showing signatures of C—O single bonds (285.8−286.7 eV), C═O double bonds (287.0−288.0 eV), and carboxylic groups (288.5−290.0 eV).[24] However, after gelation, there is a large decrease in the signal associated with C═O double bonds and, to a lesser extent, C—O single bonds, indicating significant deoxygenation. Deoxygenation after gelation, as measured by XPS, is corroborated by EDS, which gives a C/O atomic ratio of 3 for the starting GO, similar to literature reports for fully oxidized GO,[25] and a C/O ratio of 12 for the gelled sample.

The large decrease in C—O and C═O bonding shows that, in addition to causing a physical change to the GO, gelation causes a rather dramatic chemical change as well. This pronounced change in the chemical nature of the gelled GO is evident when compared to the thermally annealed sample, a so-called graphene aerogel; the shape of the carbon K-edge for the gelled sample is more similar to that of the thermally annealed gel than it is to that of the starting GO. The carbon K-edge for the gelled sample appears to have even less oxygen functionality than previously reported spectra of GO reduced either by hydrazine at 70 °C or in H_2 at 500 °C,[23] despite the fact that our reaction was carried out with simply GO and water. This significant change in the oxygen content cannot be explained solely by bonding changes along the edges of the GO sheets, but rather suggests a decrease in C—O and C═O bonding throughout the entire sheet. This is consistent with the evolution of the gel's physical appearance, which indicates that changes in bonding occur throughout the body of the GO sheets as they contract and wrinkle. Therefore, the physical and chemical changes that occur during the sol−gel transition seem to be related, as bonding within and between GO sheets is accompanied by a loss of oxygen functional groups.

Further evidence for the coupling of the chemical and physical changes during gelation can be obtained by monitoring the UV−visible absorption spectrum of GO samples reacted for different times (Figure 3). The starting GO material shows a

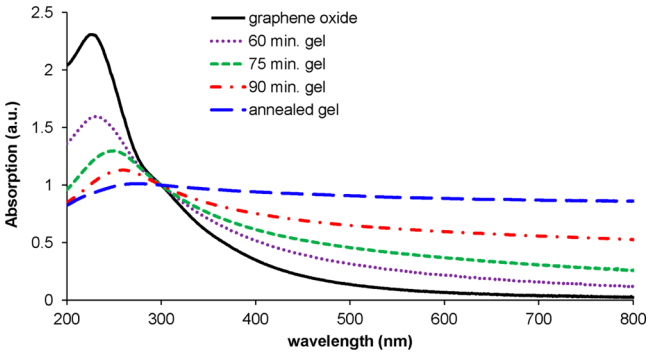

Figure 3. UV−visible absorption spectra for GO after specified reaction times and following thermal annealing, normalized at 300 nm.

large UV absorption peak at ~230 nm and a decaying absorption in the visible region, consistent with its brown color. This spectrum remains unchanged until 60 min of reaction time, when the absorption in the visible region begins to increase relative to that in the UV region. At 75 min, a shift of the peak absorption toward lower energy is also evident. After 90 min, these two important changes have developed further: (i) the peak absorption is red-shifted and (ii) the relative UV absorption is significantly decreased. In fact, absorption across the spectrum becomes quite flat after gelation, giving rise to the sample's black color. The decrease in the height of the UV absorption peak for GO has been ascribed to the loss of oxygen-containing functional groups,[26] and the peak shift to lower energy has been observed in chemically reduced GO, similar to the smaller energy gap in conjugated polymers and polycyclic aromatic molecules of increasing size.[21] As with the XPS analysis, the gelled GO has optical properties more akin to those of the annealed sample than to those of the starting GO. These changes indicate simultaneous deoxygenation and reparation of the sp^2 network during gelation, creating larger areas of conjugation to absorb across a broad range of wavelengths.[25] Furthermore, these effects occur on the same time scale as the sol−gel transition itself, suggesting that they can attributed to a single process and that this process occurs mostly between 60 and 90 min of gelation.

Following gelation, the hydrogels have remarkable thermal stability. Previous work on aerogels synthesized by this method showed enhanced stability only up to 100 °C,[14] yet the TGA results in this work (Figure 4) show that the reacted hydrogels can be heated above 500 °C in the presence of oxygen gas before experiencing thermal degradation. Unreacted GO undergoes a significant mass loss (~35%) at 200 °C. This is attributed to the loss of oxygen-containing groups in the material, as observed in previous studies of GO and GO-based xerogels.[20,26,27] Samples that were reacted for less than 60 min

dx.doi.org/10.1021/jp5092027 | J. Phys. Chem. C XXXX, XXX, XXX−XXX

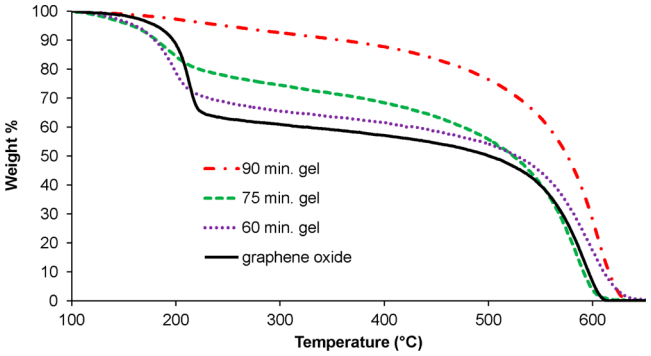

Figure 4. TGA of GO before, during, and after gelation. Mass-loss curves are normalized at 100 °C and baseline-subtracted.

show similar results to the starting material. However, the low-temperature degradation is somewhat lessened for samples reacted for 75 min, and it is completely absent for reaction times of 90 min or longer. The as-made aerogel is much more thermally stable than GO in the 200−550 °C range. The time scale of the evolving thermal properties during gelation exactly matches that of the above characterizations, which again demonstrates that the sol−gel transition requires significant deoxygenation of GO.

All of the changes described here occur concurrently between 60 and 90 min of hydrothermal reaction, indicating that they are not independent, but rather are a result of a single transformation. To demonstrate the surprising congruence of these evolving properties, the various measured parameters are plotted in Figure 5 versus sample reaction time. The position of the maximum in the UV−visible absorption spectrum (Figure 5a) shifts from 230 to 265 nm, and the relative absorption at 800 nm compared to that at 300 nm (Figure 5b) increases from ~0.02 to 0.6. The C/O ratio increases from 3 to 12 (Figure 5c), and the weight remaining after oxygen removal increases from 65% to >95% (Figure 5d). All of these changes occur on the same time scale, with the steepest change occurring around 75 min and no significant change occurring after 120 min.

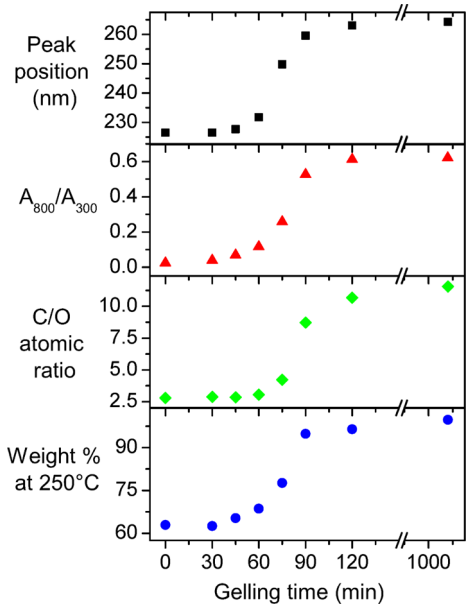

Figure 5. (a) UV−visible absorption peak position, (b) visible-to-UV absorption ratio, (c) carbon-to-oxygen ratio measured by EDS, and (d) fractional mass remaining at 250 °C measured by TGA for GO samples plotted as functions of reaction time.

Through physical, chemical, and optical characterization at various time points in the sol−gel reaction, we have shown GO undergoes the following simultaneous and dramatic changes: (1) densification and formation of a monolith; (2) change in texture from flat to wrinkled; (3) a decrease in the oxygen concentration; (4) increase in thermal stability; (5) decrease in intensity of UV light absorption, relative to visible light; and (6) shift in the UV light absorption peak. The densification and formation of a monolith, along with the wrinkling of the constituent sheets (observations 1 and 2), confirm that GO sheets are in fact bound together during gelation, causing the gel to shrink as the sheets wrinkle to form a porous structure. Observations 3−5 originate from a loss of oxygen-containing functional groups. The extent of the oxygen loss is too great to be ascribed solely to reactions at the edges of GO sheets. Therefore, the reaction is simultaneously a cross-linking between sheets and a chemical transformation within the body of the sheet, whereby oxygen is removed from the material. Although others have examined oxygen loss in fully formed hydrogels,[14] the direct time correlation between gelation and deoxygenation has never before been demonstrated.

To determine the form of oxygenated species lost from GO during gelation, we calculated the C/O ratio of the mass of oxygen-rich material during the sol−gel transition. To determine mass loss, we vacuum-filtered a volume of GO solution and compared its mass to that of the dried aerogel synthesized from the same volume. The mass loss associated with gelation was found to be approximately 44%. Combining this figure with the change in oxygen concentration after gelation by EDS, we estimate that the C/O ratio in the material removed from the GO after gelation was 0.45. This ratio indicates that a large portion of carbon is lost as CO_2 during hydrothermal gelation. Deoxygenation of GO has previously been observed in reactions of GO with strong base through loss of CO_2.[26] Although sometimes referred to as "reduction" of GO, this reaction is more appropriately regarded as disproportionation, where removal of oxygen-containing species, such as CO_2, is accompanied by electron donation to the remaining carbon material. This model matches our data more closely than other reports of deoxygenation, which found that the GO sheets shed organic molecular fragments that remain in solution.[28,29]

CONCLUSIONS

In summary, the process of converting aqueous GO suspensions to monolithic hydrogels was investigated in detail by probing their optical, chemical, thermal, and physical properties at various time points during the early stages of the reaction. The transition from a solution to a gel, in conjunction with the wrinkling of GO sheets seen by TEM, demonstrates that the sheets were cross-linked. Additionally, we found that the aerogel formed from GO sheets is chemically dissimilar from GO and has properties more consistent with those of thermally annealed, or reduced, aerogels. There is a significant loss of oxygen during gelation, and the sp^2 carbon network is partially re-formed. Finally, and most surprisingly, the changes in physical, chemical, and optical properties occur on precisely the same time scale, indicating that they share a common origin in the sol−gel transition: the binding together

dx.doi.org/10.1021/jp5092027 | J. Phys. Chem. C XXXX, XXX, XXX−XXX

of GO sheets and the accompanying loss of oxygen through carbon dioxide evolution.

Although our results offer an important insight into the dynamics of GO gelation, they do not settle the matter of whether sheets are bound covalently or through weaker forces such as $\pi-\pi$ stacking. Further investigation into the sol−gel reaction mechanism should include detailed characterization of the intermediate chemical species in the solid product, the reaction solution, and any evolved gases. Understanding the mechanism of GO gelation will allow researchers to gain separate control of both the physical properties and the oxygen content of graphene-based aerogels.

■ ASSOCIATED CONTENT

Supporting Information

Nitrogen porosimetry and Raman spectroscopy data. This material is available free of charge via the Internet at http://pubs.acs.org.

■ AUTHOR INFORMATION

Corresponding Author

*E-mail: azettl@physics.berkeley.edu.

Notes

The authors declare no competing financial interest.

■ ACKNOWLEDGMENTS

This work was supported in part by the UC Lab Fees Research Program under Award 12-LR-235323, which provided for supplies and materials and student support (A.P.G.); the Director, Office of Energy Research, Office of Basic Energy Sciences, Materials Sciences and Engineering Division, of the U.S. Department of Energy (DOE) under Contract DE-AC02-05CH11231, under the sp2-bonded Materials Program, which provided for TEM characterization; the NSF under Grant DMR-1206512, which provided for optical characterization; and Lawrence Livermore National Laboratory (LLNL) Directed Research and Development (LDRD) Grant 13-LW-099. W.M., A.M., and A.Z. received support from the Center of Integrated Nanomechanical Systems under NSF Grant EEC-0832819. Work performed at LLNL was done under the auspices of the U.S. DOE under Contract DE-AC52-07NA27344. The authors thank Anna Harley-Trochimczyk and Carlo Carraro for their assistance with XPS and Isaac G. Broaders for his motivation in expediting the completion of this research.

■ REFERENCES

(1) Biener, J.; Stadermann, M.; Suss, M.; Worsley, M. A.; Biener, M. M.; Rose, K. A.; Baumann, T. F. Advanced Carbon Aerogels for Energy Applications. *Energy Environ. Sci.* **2011**, *4*, 656−667.

(2) Lei, Z.; Lu, L.; Zhao, X. S. The Electrocapacitive Properties of Graphene Oxide Reduced by Urea. *Energy Environ. Sci.* **2012**, *5*, 6391−6399.

(3) Wu, Z.-S.; Sun, Y.; Tan, Y.-Z.; Yang, S.; Feng, X.; Müllen, K. Three-Dimensional Graphene-Based Macro- and Mesoporous Frameworks for High-Performance Electrochemical Capacitive Energy Storage. *J. Am. Chem. Soc.* **2012**, *134*, 19532−19535.

(4) Niu, Z.; Liu, L.; Zhang, L.; Chen, X. Porous Graphene Materials for Water Remediation. *Small* **2014**, *10*, 3434−3441.

(5) Yavari, F.; Chen, Z.; Thomas, A. V.; Ren, W.; Cheng, H.-M.; Koratkar, N. High Sensitivity Gas Detection Using a Macroscopic Three-Dimensional Graphene Foam Network. *Sci. Rep.* **2011**, *1*, 166.

(6) Han, S.; Wu, D.; Li, S.; Zhang, F.; Feng, X. Porous Graphene Materials for Advanced Electrochemical Energy Storage and Conversion Devices. *Adv. Mater.* **2014**, *26*, 849−864.

(7) Worsley, M. A.; Kucheyev, S. O.; Mason, H. E.; Merrill, M. D.; Mayer, B. P.; Lewicki, J.; Valdez, C. A.; Suss, M. E.; Stadermann, M.; Pauzauskie, P. J.; Satcher, J. H., Jr.; Biener, J.; Baumann, T. F. Mechanically Robust 3D Graphene Macroassembly with High Surface Area. *Chem. Commun.* **2012**, *48*, 8428−8430.

(8) Worsley, M. A.; Pauzauskie, P. J.; Olson, T. Y.; Biener, J.; Satcher, J. H.; Baumann, T. F. Synthesis of Graphene Aerogel with High Electrical Conductivity. *J. Am. Chem. Soc.* **2010**, *132*, 14067−14069.

(9) Bai, H.; Li, C.; Wang, X.; Shi, G. On the Gelation of Graphene Oxide. *J. Phys. Chem. C* **2011**, *115*, 5545−5551.

(10) Chmiola, J.; Yushin, G.; Gogotsi, Y.; Portet, C.; Simon, P.; Taberna, P. L. Anomalous Increase in Carbon Capacitance at Pore Sizes Less Than 1 Nanometer. *Science* **2006**, *313*, 1760−1763.

(11) Qiu, L.; Liu, J. Z.; Chang, S. L. Y.; Wu, Y.; Li, D. Biomimetic Superelastic Graphene-Based Cellular Monoliths. *Nat. Commun.* **2012**, *3*, 1241.

(12) Worsley, M. A.; Charnvanichborikarn, S.; Montalvo, E.; Shin, S. J.; Tylski, E. D.; Lewicki, J. P.; Nelson, A. J.; Satcher, J. H.; Biener, J.; Baumann, T. F.; Kucheyev, S. O. Toward Macroscale, Isotropic Carbons with Graphene-Sheet-Like Electrical and Mechanical Properties. *Adv. Funct. Mater.* **2014**, *24*, 4259−4264.

(13) Zhu, Y.; Murali, S.; Stoller, M. D.; Ganesh, K. J.; Cai, W.; Ferreira, P. J.; Pirkle, A.; Wallace, R. M.; Cychosz, K. A.; Thommes, M.; Su, D.; Stach, E. A.; Ruoff, R. S. Carbon-Based Supercapacitors Produced by Activation of Graphene. *Science* **2011**, *332*, 1537−1541.

(14) Xu, Y.; Sheng, K.; Li, C.; Shi, G. Self-Assembled Graphene Hydrogel via a One-Step Hydrothermal Process. *ACS Nano* **2010**, *4*, 4324−4330.

(15) Gash, A. E.; Tillotson, T. M.; Satcher, J. H., Jr; Hrubesh, L. W.; Simpson, R. L. New Sol−Gel Synthetic Route to Transition and Main-Group Metal Oxide Aerogels Using Inorganic Salt Precursors. *J. Non-Cryst. Solids* **2001**, *285*, 22−28.

(16) Mohanan, J. L.; Arachchige, I. U.; Brock, S. L. Porous Semiconductor Chalcogenide Aerogels. *Science* **2005**, *307*, 397−400.

(17) Pekala, R. W.; Alviso, C. T.; Kong, F. M.; Hulsey, S. S. Aerogels Derived from Multifunctional Organic Monomers. *J. Non-Cryst. Solids* **1992**, *145*, 90−98.

(18) Lerf, A.; He, H.; Forster, M.; Klinowski, J. Structure of Graphite Oxide Revisited. *J. Phys. Chem. B* **1998**, *102*, 4477−4482.

(19) Erickson, K.; Erni, R.; Lee, Z.; Alem, N.; Gannett, W.; Zettl, A. Determination of the Local Chemical Structure of Graphene Oxide and Reduced Graphene Oxide. *Adv. Mater.* **2010**, *22*, 4467−4472.

(20) Stankovich, S.; Dikin, D. A.; Piner, R. D.; Kohlhaas, K. A.; Kleinhammes, A.; Jia, Y.; Wu, Y.; Nguyen, S. T.; Ruoff, R. S. Synthesis of Graphene-Based Nanosheets via Chemical Reduction of Exfoliated Graphite Oxide. *Carbon* **2007**, *45*, 1558−1565.

(21) Li, D.; Müller, M. B.; Gilje, S.; Kaner, R. B.; Wallace, G. G. Processable Aqueous Dispersions of Graphene Nanosheets. *Nat. Nanotechnol.* **2008**, *3*, 101−105.

(22) Dreyer, D. R.; Park, S.; Bielawski, C. W.; Ruoff, R. S. The Chemistry of Graphene Oxide. *Chem. Soc. Rev.* **2010**, *39*, 228−240.

(23) Yang, D.; Velamakanni, A.; Bozoklu, G.; Park, S.; Stoller, M. D.; Piner, R. D.; Stankovich, S.; Jung, I.; Field, D. A.; Ventrice, C. A., Jr.; Ruoff, R. A. Chemical Analysis of Graphene Oxide Films after Heat and Chemical Treatments by X-ray Photoelectron and Micro-Raman Spectroscopy. *Carbon* **2009**, *47*, 145−152.

(24) Yumitori, S. Correlation of C1s Chemical State Intensities with the O1s Intensity in the XPS Analysis of Anodically Oxidized Glass-Like Carbon Samples. *J. Mater. Sci.* **2000**, *35*, 139−146.

(25) Dimiev, A.; Kosynkin, D. V.; Alemany, L. B.; Chaguine, P.; Tour, J. M. Pristine Graphite Oxide. *J. Am. Chem. Soc.* **2012**, *134*, 2815−2822.

(26) Dimiev, A. M.; Alemany, L. B.; Tour, J. M. Graphene Oxide. Origin of Acidity, Its Instability in Water, and a New Dynamic Structural Model. *ACS Nano* **2013**, *7*, 576−588.

(27) Jiao, T.; Wang, Y.; Zhang, Q.; Yan, X.; Zhao, X.; Zhou, J.; Gao, F. Self-Assembly and Headgroup Effect in Nanostructured Organogels via Cationic Amphiphile-Graphene Oxide Composites. *PLoS One* **2014**, *9*, e101620.
(28) Rourke, J. P.; Pandey, P. A.; Moore, J. J.; Bates, M.; Kinloch, I. A.; Young, R. J.; Wilson, N. R. The Real Graphene Oxide Revealed: Stripping the Oxidative Debris from the Graphene-like Sheets. *Angew. Chem., Int. Ed.* **2011**, *50*, 3173−3177.
(29) Thomas, H. R.; Day, S. P.; Woodruff, W. E.; Valles, C.; Young, R. J.; Kinloch, I. A.; Morley, G. W.; Hanna, J. V.; Wilson, N. R.; Rourke, J. P. Deoxygenation of Graphene Oxide: Reduction or Cleaning? *Chem. Mater.* **2013**, *25*, 3580−3588.